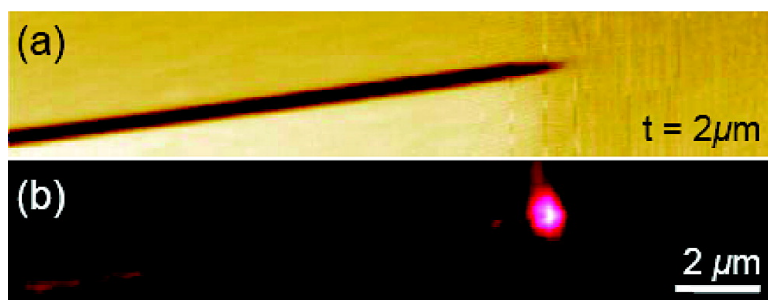


Nanofocusing with Channel Plasmon Polaritons

Valentyn S. Volkov, Sergey I. Bozhevolnyi, Sergio G. Rodrigo, Luis Marti#n-Moreno, Francisco J. Garc#i#a-Vidal, Eloi#se Devaux, and Thomas W. Ebbesen

Nano Lett., 2009, 9 (3), 1278-1282 • DOI: 10.1021/nl900268v • Publication Date (Web): 16 February 2009

Downloaded from <http://pubs.acs.org> on March 13, 2009



More About This Article

Additional resources and features associated with this article are available within the HTML version:

- Supporting Information
- Access to high resolution figures
- Links to articles and content related to this article
- Copyright permission to reproduce figures and/or text from this article

[View the Full Text HTML](#)

Nanofocusing with Channel Plasmon Polaritons

Valentyn S. Volkov,[†] Sergey I. Bozhevolnyi,^{*,†} Sergio G. Rodrigo,[‡]
Luis Martín-Moreno,[‡] Francisco J. García-Vidal,[§] Eloïse Devaux,^{||}
and Thomas W. Ebbesen^{||}

Institute of Sensors, Signals and Electrotechnics (SENSE), University of Southern Denmark, Niels Bohrs Allé 1, DK-5230 Odense M, Denmark, Instituto de Ciencia de Materiales de Aragón and Departamento de Física de la Materia Condensada, CSIC—Universidad de Zaragoza, E-50009 Zaragoza, Spain, Departamento de Física Teórica de la Materia Condensada, Universidad Autónoma de Madrid, E-28049 Madrid, Spain, and ISIS, CNRS UMR 7006, Université Louis Pasteur, 8 allée Monge, BP 70028, 67083 Strasbourg, France

Received January 26, 2009; Revised Manuscript Received February 9, 2009

ABSTRACT

We investigate radiation nanofocusing with channel plasmon polaritons (CPPs) propagating along subwavelength metal grooves that are tapered synchronously in depth and in width. Efficient CPP nanofocusing at telecom wavelengths with the estimated field intensity enhancement of up to ~ 90 is directly demonstrated using near-field microscopy. Experimental observations are concurred with electromagnetic simulations, predicting the possibility of reaching the intensity enhancements of ~ 1200 and opening thereby exciting perspectives for practical applications of CPP nanofocusing.

Nanoguiding and concentrating of optical radiation with surface plasmon (SP) modes supported by metal nanostructures is the strategic research direction in plasmonics^{1,2} with implications ranging from quantum optics³ to nanosensing.⁴ Various configurations have been suggested for SP nanofocusing,^{5–10} all supporting progressively stronger confined SP modes in the limit of infinitely small waveguide cross sections. However, experimental demonstrations of SP nanofocusing^{11,12} have so far been indirect (based on far-field observations of scattered¹¹ or frequency upconverted¹² radiation) and inconclusive with respect to the field enhancement achieved in the focus. Here we report on design, fabrication, characterization, and modeling of radiation nanofocusing with channel plasmon polaritons (CPPs)^{13,14} that propagate along subwavelength metal grooves being gradually tapered synchronously in depth and in width. Efficient CPP nanofocusing at telecom wavelengths with the estimated field intensity enhancement of up to ~ 90 is directly demonstrated using near-field microscopy, opening thereby exciting

perspectives for practical applications of the CPP-based nanofocusing phenomenon.

The idea of radiation (nano) focusing (and thereby greatly enhancing electromagnetic fields) by gradually decreasing a waveguide cross section has always been very appealing due to its apparent simplicity. Its realization however requires for the corresponding waveguide mode to scale in size along with the waveguide cross section, a nontrivial characteristic that is not readily accessible and, for example, cannot be achieved with dielectric waveguides due to the diffraction limit. The physics of SP guiding is fundamentally different and intimately connected with the hybrid nature of SP modes, in which electromagnetic fields in dielectrics are coupled to free electron oscillations in metals.¹⁵ Several SP guiding configurations exhibit, in the limit of infinitely small waveguide dimensions, the required scale invariance, i.e., the mode size scaling linearly with that of the waveguide. The appropriate SP modes are supported, for example, by thin metal films (short-range SPs) and narrow gaps between metal surfaces (gap SPs),¹⁶ and by corresponding cylindrical, i.e., rod and coaxial, structures.^{17,18} Note that their nanofocusing^{5–9} is conceptually simple only at a fairly basic level and requires dealing with several rather complicated issues, such as excitation of the proper SP mode¹¹ and balancing between SP propagation losses (that increase for smaller waveguide cross sections) and focusing effects.^{19,20}

* Corresponding author, seib@sense.sdu.dk.

[†] Institute of Sensors, Signals and Electrotechnics (SENSE), University of Southern Denmark.

[‡] Instituto de Ciencia de Materiales de Aragón and Departamento de Física de la Materia Condensada, CSIC—Universidad de Zaragoza.

[§] Departamento de Física Teórica de la Materia Condensada, Universidad Autónoma de Madrid.

^{||} ISIS, CNRS UMR 7006, Université Louis Pasteur.

The situation becomes even more complicated if one considers SP modes whose scaling behavior is not straightforward. Thus CPP guides, which can be efficiently excited with optical fibers and used for ultracompact plasmonic components,¹⁴ exhibit rather complicated behavior with respect to their geometrical parameters,²¹ and their potential for nanofocusing of radiation has not yet been explored. We approach the problem of CPP nanofocusing by making use of the recently obtained (approximate) expression for the normalized (CPP-based) waveguide parameter²²

$$V_{\text{CPP}} \cong 2\sqrt{\frac{k_0 d \varepsilon_d \sqrt{|\varepsilon_d - \varepsilon_m|}}{|\varepsilon_m| \tan(\theta/2)}} \cong 4d\sqrt{\frac{\pi \varepsilon_d \sqrt{|\varepsilon_d - \varepsilon_m|}}{\lambda w |\varepsilon_m|}} \quad (1)$$

λ is the light wavelength ($k_0 = 2\pi/\lambda$), d and w are the V-groove depth and width, θ is the groove angle so that $\tan(\theta/2) = 0.5w/d$, ε_d and ε_m are the dielectric constants of dielectric and metal. It has been demonstrated²² that V-grooves with different dimensions and operating at different wavelengths but having the same parameter V_{CPP} feature very similar field confinement.²³ With this in mind, we came up with the idea of CPP nanofocusing by gradually decreasing the groove depth while synchronously decreasing its angle so that the corresponding waveguide parameter (eq 1) would be kept constant. In this case (and within the same approximation²²), one can show that the CPP effective index of nanometer-sized V-grooves diverges toward the taper end: $N_{\text{CPP}} \sim (k_0 d)^{-1}$; i.e., it behaves in the same manner as that of the SPP mode of a tapered nanowire.⁷ In the adiabatic approximation, the CPP field is continuously squeezed by walls of a tapered V-groove with the maximum field being limited only by the CPP propagation loss. In general, similarly to the nanofocusing with nanowires,^{19,20} the field enhancement at the taper end is a result of the interplay between CPP dissipation (contributed to by CPP absorption, reflection, and out-of-plane scattering) and field squeezing.

For the experimental verification of our idea, we have fabricated, using focused ion beam (FIB) milling, in a 1.8 μm thick gold layer (deposited on a glass substrate coated with ITO) several straight 150 μm long V-grooves with the angles close to 28° and depths of 1.1–1.3 μm , which were gradually tapered out over different distances $t = 2, 3, 4,$ and $6 \mu\text{m}$. The tapering was realized by decreasing, gradually and linearly with respect to the length of the tapered part, the number of pixels representing the groove width in the taper region while maintaining the dwell time. Making cross cuts with the FIB, we have checked that such a milling procedure results indeed in simultaneous decreasing the groove depth and angle (Figure 1a). The fabricated structures were characterized with a collection scanning near-field optical microscope (SNOM)²⁴ having an uncoated fiber tip used as a probe and an arrangement for end-fire coupling of tunable ($\lambda = 1425\text{--}1620 \text{ nm}$) TE-polarized (the electric field is parallel to the sample surface plane) radiation into a groove by positioning a tapered-lensed polarization-maintaining single-mode fiber.¹⁴ The track of the propagating radiation (distinguishable for all structures and wavelengths) featured,

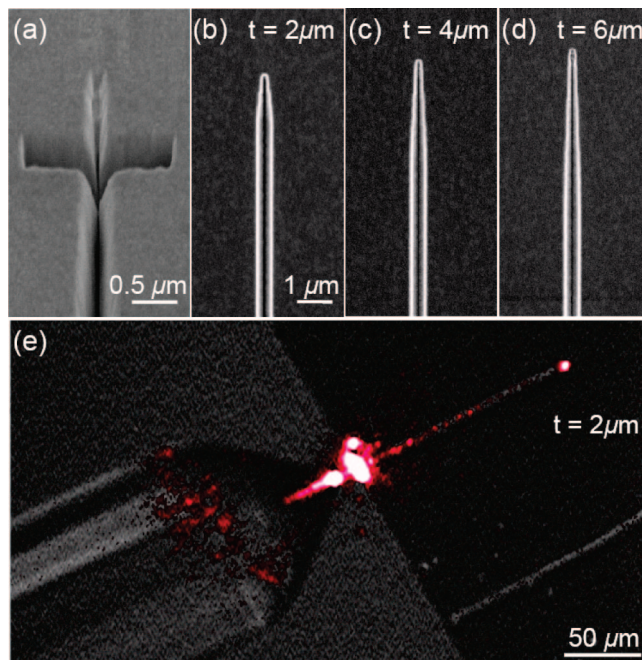


Figure 1. Tapered V-grooves. (a) SEM image of a tapered V-groove cut in the taper region to reveal a decrease in the groove angle toward the taper end. SEM images of fabricated tapered V-grooves having different taper lengths: (b) 2, (c) 4, and (d) 6 μm . (e) Microscope image of a coupling arrangement superimposed with the far-field image taken at the excitation wavelength $\lambda = 1480 \text{ nm}$ with an infrared camera, showing the track of CPP propagation and a bright spot at the 2 μm long taper.

apart from a gradual decay in visibility with the propagation distance, a rather bright spot at its termination (Figure 1e). Following the far-field adjustment, the whole fiber-sample arrangement was moved under the SNOM head for near-field mapping of the CPP intensity distribution in the structure under investigation by the uncoated sharp fiber tip of the SNOM. The tip was scanned along the sample surface at a constant distance of a few nanometers maintained by shear force feedback, and the radiation collected by the fiber was detected with a femtowatt InGaAs photoreceiver.

Our SNOM investigations showed that all fabricated structures exhibited the effect of signal enhancement at the taper end, with the near-field optical images featuring sub-wavelength-sized bright spots located at the taper end as judged from the (simultaneously recorded) topographical images (Figure 2a,b). The most remarkable enhancement effect was observed for the 2 and 3 μm long tapers (Figure 2c,d). Using the exponential fit to the optical signal variation along the CPP propagation for different tapered V-grooves excited at the wavelength of 1480 nm, we evaluated the CPP propagation length of $\sim 40 \mu\text{m}$, which is consistent with the previous observations,¹⁴ and the signal enhancement Γ defined as the ratio between the maximum signal and that expected to be at the taper end coordinate in its absence (Figure 2e). We should emphasize that the relationship between near-field optical signal distributions and field intensity distributions existing near the sample surface (in the absence of a SNOM probe) is very complicated.²⁵ Even in a very simple approximation of the dipole-like detection

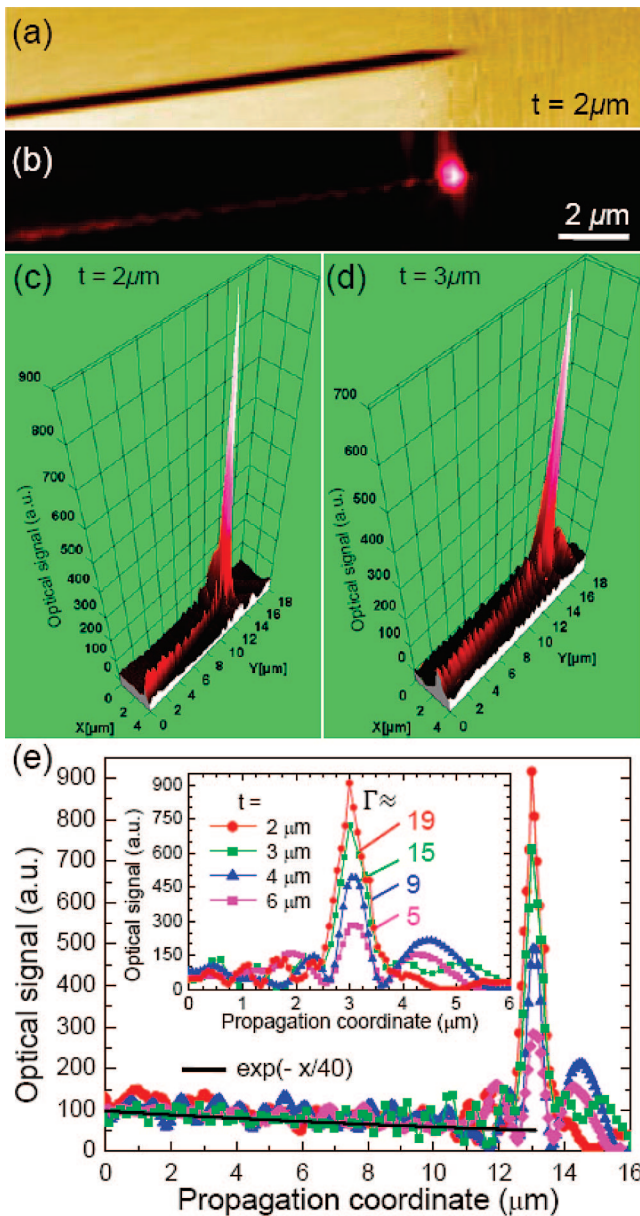


Figure 2. Plasmonic candle. (a) Topographical and (b, c) near-field optical ($\lambda = 1480$ nm) SNOM images shown in different presentations to emphasize the signal enhancement Γ realized at the taper end. (d) Optical SNOM image obtained with the $3 \mu\text{m}$ long taper. (e) Normalized cross sections obtained with optical images similar to those shown in (c) and (d) recorded for the tapered V-grooves with different taper lengths.

(taking place at the position of an effective detection point inside a fiber probe),²⁶ different field components contribute differently to the detected signal, making it impossible to directly relate the near-field intensity distributions and the corresponding SNOM images. In this situation, it is extremely important to control that the detected signal does originate from the evanescent field components (and thereby is associated with the focused CPP fields), since the detection of propagating waves, such as scattered at the taper, is much more efficient than that of evanescent ones.²⁶

Near-field optical images were recorded with shear force feedback, a few nanometers away from the surface, and then with the SNOM fiber probe scanning along a plane located

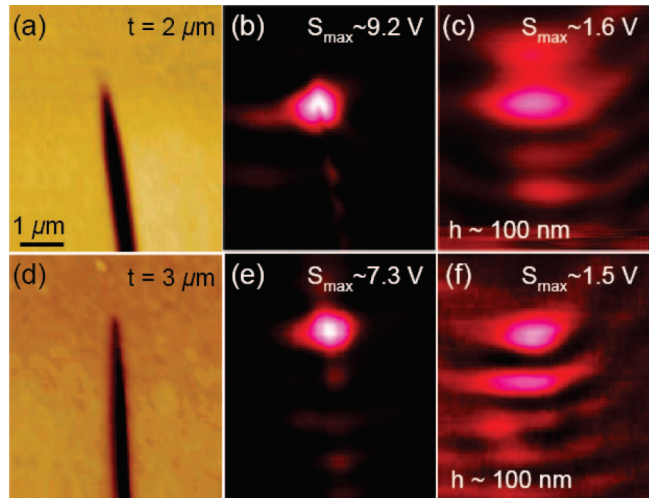


Figure 3. Influence of evanescent field components. (a, d) Topographical and near-field optical ($\lambda = 1480$ nm) SNOM images taken (b, e) with shear force feedback and (c, f) at 100 nm distance from the sample surface with the tapered V-grooves having different taper lengths: (a, b, c) 2 and (d, e, f) $3 \mu\text{m}$. The decrease in signal and the significant image blurring when increasing the probe–surface distance reveal the dominance of evanescent field components in the images obtained.

~ 100 nm from the sample surface (Figure 3). A drastic signal decrease and significant image blurring observed with the increase of the probe–surface distance signify unambiguously that the bright spots seen on the SNOM images are indeed the result of detection of evanescent (CPP) field components. It is further seen that, for the $2 \mu\text{m}$ long taper, the maximum optical signal (at the bright spot) decreased by a factor of ~ 6 (cf. Figure 3, panels b and c) while the CPP-related signal measured away from the taper region decreased only by a factor of ~ 2 . It is reasonable to assume that, in both cases, the optical signals being proportional to the field intensity (at an effective detection point²⁶) decrease exponentially with the probe–surface distance but at different rates, because the corresponding optical fields are laterally confined to the different widths. The latter implies that the observed intensity enhancement decreases also exponentially with the height of the observation plane. Finally, taking into account the circumstance that the effective detection point is located typically ~ 150 nm away from the tip end,²⁶ we obtained ~ 90 as a ballpark estimate of the field intensity enhancement realized at the sample surface with the $2 \mu\text{m}$ long taper.

In order to gain further insight and reveal the potential of CPP nanofocusing, we have conducted three-dimensional (3D) finite-difference time-domain (FDTD) simulations (using the procedure described elsewhere¹⁰) for V-grooves terminated with tapers of different lengths. In the considered configuration, the metal (gold) surface is deforming from the straight channel geometry to a flat surface in a continuous way along the mode propagation direction, i.e., along the Z axis (Figure 4a). In other words, the channel parameters being kept constant ($d_0 = 1 \mu\text{m}$, $\phi_0 = 28^\circ$, $w_0 \cong 450$ nm) during the initial $2 \mu\text{m}$ long propagation become functions of the z coordinate. We considered linear tapering with respect to the groove depth:

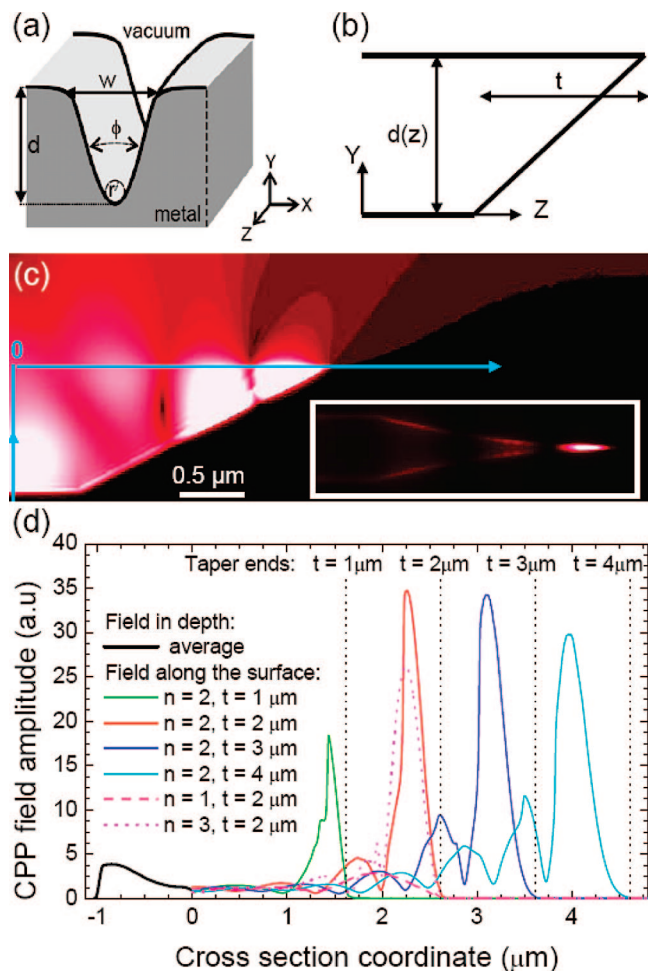


Figure 4. Simulations of CPP nanofocusing. (a) Schematic of V-groove geometry and (b) the taper region. (c) Field magnitude distribution ($x = 0$) calculated using 3D FDTD simulations of the CPP propagation ($\lambda = 1480$ nm) and focusing with the $2 \mu\text{m}$ long taper in which the groove width and depth decrease in accordance with the dependence described with $n = 2$. An inset shows the corresponding field magnitude distribution in the sample surface plane. (d) Cross sections of the field amplitude distributions along the line shown in (c) for different taper lengths and groove width–depth dependences.

$d(z) = d_0\{1 - (z - z_0)/t\}$, where t is the taper length, z_0 is the starting coordinate of the taper, and $z_0 < z < z_0 + t$ (Figure 4b). At the same time, the groove width was adjusted following three different dependencies: $w(z) = w_0(d(z)/d_0)^n$, $n = 1, 2$, and 3 . Consequently, the normalized waveguide parameter introduced in eq 1 varied as follows: $V_{\text{CPP}}(z) = V_{\text{CPP}}^0\{d_0/d(z)\}^{0.5n-1}$, so as the channel tip is approached, the parameter V was maintained constant for $n = 2$, while $V \rightarrow 0$ for $n = 1$ (constant-angle tapering) and $V \rightarrow \infty$ for $n = 3$. The simulations were performed at $\lambda = 1480$ nm in continuous-wave mode for different taper lengths in the range from 1 to $4 \mu\text{m}$. The best (with respect to the field enhancement achieved at the taper end) performance for a given taper length was found for $n = 2$ as expected, with the optimum taper length $t = 2 \mu\text{m}$ (Figure 4c,d). We believe that the optimum taper length is mainly related to constructive interference of the propagating (toward the taper)

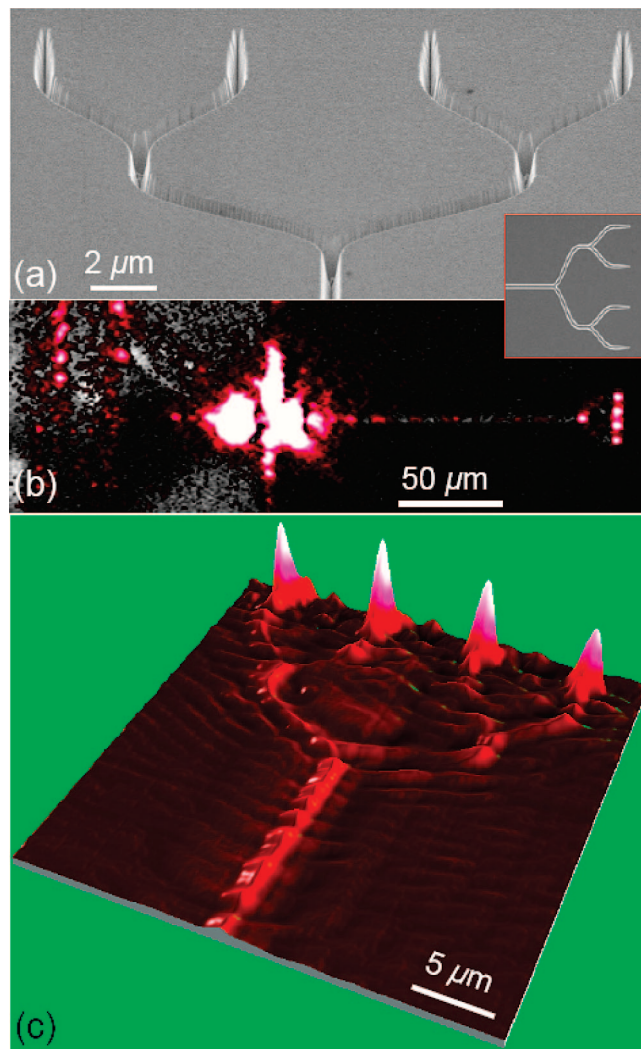


Figure 5. Plasmonic candlestick. (a) SEM image of a multichannel configuration for delivering nanofocused and enhanced radiation to four spatial locations via consecutive $5 \mu\text{m}$ long Y-splitters terminated with $2 \mu\text{m}$ long tapers (see the inset with an overview SEM image). (b) Microscope image of a coupling arrangement superimposed with the far-field image taken at the excitation wavelength $\lambda = 1500$ nm with an infrared camera, showing the track of CPP propagation and four bright spots at the tapers. (c) Near-field optical ($\lambda = 1,500$ nm) SNOM image demonstrating significant signal enhancements realized at the four groove tapers, with signal levels being similar and exceeding greatly even the signal level at the input channel.

and reflected CPP modes, though it is affected by the CPP propagation loss as well.

The theoretical findings agree well with our qualitative considerations in the sense that the groove tapering should be conducted so that the groove depth and width decrease in accord keeping the normalized CPP parameter (eq 1) constant. The simulation results are also consistent with the experimental observations, which feature the strongest enhancement for the $2 \mu\text{m}$ long taper, the occurrence of a very bright spot in near-field optical images, and the interference fringes indicating the CPP reflection and scattering in the taper region (cf. Figures 3 and 4c). At the same time, the field enhancement as estimated from the calcula-

tions is much larger than even the ballpark estimate. Indeed, using the same definition as before one obtains (Figure 4d) the field intensity enhancement of ~ 1200 for the $2\ \mu\text{m}$ long taper with $n = 2$. On the other hand, some difference should be expected given the limited FIB resolution and the fact that the maximum field intensity is calculated to be fairly close to the taper end with the taper width being only ~ 50 nm (while the groove depth is still ~ 300 nm). Considering the potential of CPP nanofocusing, further simulations are needed in order to elucidate the influence of all parameters (i.e., the initial groove angle and waveguide parameter) on the resulting effect of field enhancement.

In conclusion, we have suggested a new avenue for radiation nanofocusing, viz., by utilizing the CPP guiding along subwavelength metal grooves whose depth and width decrease in accord maintaining the waveguide parameter and, thereby, the degree of field confinement. One can envisage further development of this concept for other plasmonic waveguides based on gap SP modes²² as well as with respect to applications for miniature biosensors by advantageously exploiting the fact the CPP-based nanophotonic circuits have been found performing exceptionally well.^{2,14} Thus we explored the prospect of realization of a multichannel configuration for delivering nanofocused and enhanced CPP fields to several different spatial locations by making use of consecutive Y-splitters (Figure 5). The level of signal enhancement observed with the SNOM images was fairly constant for the four tapers amounting to a factor of ~ 5 with respect to the signal at the input channel, which is consistent with the enhancement of ~ 20 observed for the individual $2\ \mu\text{m}$ long taper (Figure 2c), given the power distribution between four channels. This experiment demonstrates that the suggested approach for radiation nanofocusing is rather versatile and robust, features that are extremely important and indispensable for future applications.

References

- (1) Lal, S.; Link, S.; Halas, N. J. *Nat. Photonics* **2007**, *1*, 641–648.
- (2) Ebbesen, T. W.; Genet, C.; Bozhevolnyi, S. I. *Phys. Today* **2008**, *61*, 44–50.
- (3) Chang, D. E.; Sørensen, A. S.; Demler, E. A.; Lukin, M. D. *Nat. Phys.* **2007**, *3*, 807–812.
- (4) Ringler, M.; Schwemer, A.; Wunderlich, M.; Nichtl, A.; Kürzinger, K.; Klar, T. A.; Feldmann, J. *Phys. Rev. Lett.* **2008**, *100*, 203002.
- (5) Nerkararyan, K. V. *Phys. Lett. A* **1997**, *237*, 103–105.
- (6) Babadjanyan, A. J.; Margaryan, N. L.; Nerkararyan, K. V. *J. Appl. Phys.* **2000**, *87*, 3785–3788.
- (7) Stockman, M. I. *Phys. Rev. Lett.* **2004**, *93*, 137404.
- (8) Gramotnev, D. K. *J. Appl. Phys.* **2005**, *98*, 104302.
- (9) Vernon, K.; Gramotnev, D. K.; Pile, D. F. P. *J. Appl. Phys.* **2007**, *101*, 104312.
- (10) Moreno, E.; Rodrigo, S. G.; Bozhevolnyi, S. I.; Martín-Moreno, L.; García-Vidal, F. J. *Phys. Rev. Lett.* **2008**, *100*, 023901.
- (11) Ropers, C.; Neacsu, C. C.; Elsaesser, T.; Albrecht, M.; Raschke, M. B.; Lienau, C. *Nano Lett.* **2007**, *7*, 2784–2788.
- (12) Verhagen, E.; Polman, A.; Kuipers, L. *Opt. Express* **2008**, *16*, 45–57.
- (13) Novikov, I. V.; Maradudin, A. A. *Phys. Rev. B* **2002**, *66*, 035403.
- (14) Bozhevolnyi, S. I.; Volkov, V. S.; Devaux, E.; Laluet, J.-Y.; Ebbesen, T. W. *Nature* **2006**, *440*, 508.
- (15) Raether, H. *Surface Plasmons*; Springer-Verlag: Berlin, 1988.
- (16) Economou, E. N. *Phys. Rev.* **1969**, *182*, 539–554.
- (17) Pfeiffer, C. A.; Economou, E. N.; Ngai, K. L. *Phys. Rev. B* **1974**, *10*, 3038–3051.
- (18) Takahara, J.; Yamagishi, S.; Taki, H.; Morimoto, A.; Kobayashi, T. *Opt. Lett.* **1997**, *22*, 475–477.
- (19) Ding, W.; Andrews, S. R.; Maier, S. A. *Phys. Rev. A* **2007**, *75*, 063822.
- (20) Gramotnev, D. K.; Vogel, M. W.; Stockman, M. I. *J. Appl. Phys.* **2008**, *104*, 034311.
- (21) Moreno, E.; García-Vidal, F. J.; Rodrigo, S. G.; Martín-Moreno, L.; Bozhevolnyi, S. I. *Opt. Lett.* **2006**, *31*, 3447–3449.
- (22) Bozhevolnyi, S. I.; Jung, J. *Opt. Express* **2008**, *16*, 2676–2684.
- (23) The normalized waveguide parameter (normalized frequency) in the form $V = k_0 w (\epsilon_f - \epsilon_s)^{0.5}$, w being the film thickness and ϵ_f and ϵ_s the dielectric constants of the film and the substrate, was previously used for planar thin-film waveguides (Kogelnik, H.; Ramaswamy, V. *Appl. Opt.* **1974**, *13*, 1857–1862) as a basic parameter that along with the asymmetry parameter allowed charting universal dispersion curves for TE modes.
- (24) DME-DualScope, Herlev, Denmark.
- (25) Bozhevolnyi, S. I.; Vohnsen, B.; Bozhevolnaya, E. A. *Opt. Commun.* **1999**, *172*, 171–179.
- (26) Radko, I. P.; Bozhevolnyi, S. I.; Gregersen, N. *Appl. Opt.* **2006**, *45*, 4054–4061.

NL900268V